

Finite-size scaling of coherence and steered coherence in the Lipkin-Meshkov-Glick model

Ming-Liang Hu,^{1,2,*} Fan Fang,³ and Heng Fan^{2,4,5,†}

¹*School of Science, Xi'an University of Posts and Telecommunications, Xi'an 710121, China*

²*Institute of Physics, Chinese Academy of Sciences, Beijing 100190, China*

³*School of Electronic Engineering, Xi'an University of Posts and Telecommunications, Xi'an 710121, China*

⁴*CAS Center for Excellence in Topological Quantum Computation, University of Chinese Academy of Sciences, Beijing 100190, China*

⁵*Songshan Lake Materials Laboratory, Dongguan 523808, China*

Quantum coherence reflects the origin of quantumness and might be capable of extracting the subtle nature of a system. We investigate the ground-state coherence and steered coherence in the Lipkin-Meshkov-Glick model and show that they detect faithfully the quantum phase transitions of this model. Moreover, we carry out scaling analysis on the coherence and steered coherence by means of the continuous unitary transformation method and it is found that the scaling exponents are uniquely determined by the phase region of this model. These results may provide useful insights into the mechanism underlying quantum criticality in many-body systems.

PACS numbers: 03.65.Yz, 64.70.Tg, 75.10.Pq;

I. INTRODUCTION

Quantum phase transition (QPT) is a purely quantum phenomenon which originates from quantum fluctuations [1]. Besides the traditional method, it has also been widely studied by virtue of concepts borrowed from quantum information theory in the past two decades. To be specific, this is mainly carried out based on singular behaviors of the variety of quantum correlations. For example, the ground-state entanglement of two carefully chosen sublattices or two neighboring spins spotlight successfully the QPTs of certain spin models [2–6]. Additionally, the quantum discord of two spins can also cleanly signal the QPTs in some one-dimensional spin chain models [7–10]; in particular, it signals the QPTs of the Heisenberg XXZ model even at finite temperatures [9].

As the origin of quantumness and the fundamental property of quantum states not available in classical physics, quantum coherence remains one of the research focuses of the quantum theory since the beginning of the 20th century and it may underlie the singularity of quantum critical behaviors of various many-body systems. In particular, since the formulation of the resource theory of coherence [10–12], the study of QPTs from the perspective of the ground-state coherence has been given more attention due to its fundamentality. In fact, its feasibility has been validated through studying those one-dimensional spin models, including the spin-1/2 Ising and XX models [13], the XY model [14–17], the general XYZ model [18], as well as the spin-1 XXZ model [19].

Starting from the coherence measures, one can not only interpret those already known quantum correlations [20–24] but also introduce other quantifiers of quantumness [25–29]. One of these coherence-based quantifiers is the steered coherence for a bipartite state ρ_{AB} , including the average steered coherence (ASC) with respect to the mutually unbiased bases [25–27] and the maximal steered coherence (MSC) in the eigenba-

sis of $\rho_B = \text{tr}_A \rho_{AB}$ [29]. The feasibility of the ASC in signaling QPTs has been validated for certain spin systems [30, 31], and compared with entanglement and quantum discord, it has the benefit of being long ranged, thus releases the strict restriction on the choice of special spins for probing QPTs.

While the above works are mainly on the one-dimensional systems, the coherence in the high-dimensional systems might exhibit richer phenomena due to their high coordinate number. One of these models is the Lipkin-Meshkov-Glick (LMG) model. It was first introduced in nuclear physics [32–34] and more recent studies showed that it can be simulated in trapped ions [35, 36], nitrogen-vacancy center ensembles [37], and superconducting qubits [38]. It has also found applications in quantum information processing [39, 40]. For these reasons, we investigate coherence and steered coherence in the LMG model with emphasis on their capability to characterize the quantum criticality. We consider the following three cases: (i) the thermodynamic limit case by means of the semiclassical approach, (ii) the isotropic case which is exactly solvable with arbitrary system size N , and (iii) the anisotropic case by utilizing the continuous unitary transformation (CUT) technique [41, 42]. The results show that both the coherence and steered coherence detect QPT of the LMG model faithfully, and their dependence on the system size is found to be scaled with different exponents in different phases. These observations show a robust pathway to explore quantum criticality in many-body systems by the coherence based indicators.

The structure of this paper is as follows. In Sec. II, we recall some preliminaries on quantifying coherence and steered coherence, then in Sec. III, we present their solutions for the LMG model. Sec. IV is devoted to analyzing their behaviors and their scaling exponents in different phase regions. Finally, we summarize the main results in Sec. V.

II. PRELIMINARIES

In this section we recall briefly two measures of coherence defined within the resource theoretic framework and the related quantification of steered coherence. For a state described

*Electronic address: mingliang0301@163.com

†Electronic address: hfan@iphy.ac.cn

by the density operator ρ , we consider its l_1 norm of coherence and relative entropy of coherence given by [11]

$$C_{l_1}^{(|i\rangle)}(\rho) = \sum_{i \neq j} |\rho_{ij}|, \quad C_r^{(|i\rangle)}(\rho) = S(\rho_{\text{diag}}) - S(\rho), \quad (1)$$

where the subscripts l_1 and r indicate that the metrics are the l_1 norm and relative entropy, respectively, while the superscript $\{|i\rangle\}$ indicates the reference basis in which the coherence is defined. Moreover, ρ_{ij} denotes the elements of ρ in the reference basis $\{|i\rangle\}$, ρ_{diag} is an operator obtained from ρ by replacing all its off-diagonal elements with zero, $S(\rho) = -\text{tr}(\rho \log_2 \rho)$ is the von Neumann entropy of ρ , and likewise for $S(\rho_{\text{diag}})$.

Starting from the above coherence measures, one can then consider the steered coherence for a two-qubit state ρ_{AB} , with qubit A (B) holding by Alice (Bob). There are two frameworks for such a problem. Within the first framework, it was formulated by considering the three mutually unbiased observables $\{\sigma_{x,y,z}\}$ (i.e., the Pauli operators). Specifically, Alice first measures σ_i on qubit A and then informs Bob of her choice σ_i and outcome a , based on which Bob measures the average coherence of the collapsed states of qubit B with respect to the eigenbases of the two $\sigma_j \neq \sigma_i$ (as two different spin directions cannot be measured simultaneously in experiments, this could be achieved by Bob's randomly chosen eigenbases of the two $\sigma_j \neq \sigma_i$ with equal probability for every round of Alice's measurements). After many rounds of Alice's local measurements of $\{\sigma_{x,y,z}\}$ with equal probability and the classical communication between Alice and Bob, the ASC of qubit B will be given by [25]

$$C_\alpha^{\text{asc}}(\rho_{AB}) = \frac{1}{2} \sum_{i \neq j, a} p_{\Pi_i^a} C_\alpha^{\sigma_j}(\rho_{B|\Pi_i^a}), \quad (2)$$

where $p_{\Pi_i^a} = \text{tr}(\Pi_i^a \rho_{AB})$ defines the probability of Alice's outcome a when she measures σ_i , $\rho_{B|\Pi_i^a} = \text{tr}_A(\Pi_i^a \rho_{AB}) / p_{\Pi_i^a}$ is the collapsed state of B , $\Pi_i^\pm = (\mathbb{1} \pm \sigma_i)/2$ is the measurement operator ($\mathbb{1}$ is the 2×2 identity operator), and $\alpha = l_1$ or r . When $C_\alpha^{\text{asc}}(\rho_{AB})$ is larger than a threshold (i.e., the tight upper bound of the sum of the single-qubit coherences in the three mutually unbiased bases), it is said that there is a nonlocal advantage of quantum coherence (NAQC). In Ref. [25], the authors showed that the separable ρ_{AB} can never achieve the NAQC, that is, the states achieving the NAQC form a subset of the entangled states. This observation also holds for the $(d \times d)$ -dimensional states [26]. In this sense, one may view what the NAQC captures as a kind of bipartite quantum correlation stronger than entanglement.

The second framework refers to the steered coherence on B with respect to the eigenbasis $\mathcal{B} = \{|\xi_i\rangle\}$ of $\rho_B = \text{tr}_A \rho_{AB}$. To be explicit, Alice first performs the positive-operator-valued measurements (POVM) M on her qubit A ; Bob then measures the coherence of $\rho_{B|M} = \text{tr}_A(M \rho_{AB}) / p_M$ in the basis \mathcal{B} , where $p_M = \text{tr}(M \rho_{AB})$. The MSC on qubit B can be written as [29]

$$C_\alpha^{\text{msc}}(\rho_{AB}) = \inf_{\mathcal{B}} \left\{ \max_{M \in \text{POVM}} C_\alpha^{\mathcal{B}}(\rho_{B|M}) \right\}, \quad (3)$$

where the infimum over \mathcal{B} is necessary only when ρ_B is degenerate. $C_\alpha^{\text{msc}}(\rho_{AB})$ is also intimately related to quantum correla-

tions, e.g., it is maximal for any pure entangled state with full Schmidt rank and vanishes for quantum-classical states [29].

The reasons we consider the coherence based indicators are as follows. First, quantum coherence underlies entanglement and discord, which have brought new insights to QPTs, thus it is quite likely that the coherence based indicators would signal the QPTs. Second, they are analytically solvable, whereas the calculation of discord is rather more involved [7]. Finally, the critical points captured by discord do not always correspond to QPTs as they may stem from the sudden change of the optimal measurement basis in its definition [7]; thus it is necessary to seek complementary indicators of QPTs.

III. SOLUTION OF COHERENCE AND STEERED COHERENCE FOR THE LMG MODEL

Spin system is a natural playground for revealing quantum characteristics and is also a candidate for building blocks implementing quantum computation and information processing tasks. The LMG model characterizes a system consisting of N spin-1/2 particles that are mutually interacted with each other. The Hamiltonian (in units of \hbar) reads [41, 42]

$$\begin{aligned} \hat{H} &= -\frac{\lambda}{N} \sum_{i < j} (\sigma_x^i \sigma_x^j + \gamma \sigma_y^i \sigma_y^j) - h \sum_i \sigma_z^i \\ &= -\frac{2\lambda}{N} (S_x^2 + \gamma S_y^2) - 2h S_z + \frac{\lambda}{2} (1 + \gamma), \end{aligned} \quad (4)$$

where σ_v^i ($v = x, y, z$) represents the Pauli operators at site i , λ characterizes the spin interaction (with γ being its anisotropy in the xy plane), and the prefactor $1/N$ is introduced for eliminating infinity of the free energy per spin in the thermodynamic limit. Moreover, h is the transverse magnetic field and $S_v = \sum_i \sigma_v^i / 2$. In the following, we concentrate on the ferromagnetic case and we set $\lambda = 1$ (i.e., h will be in units of λ), $0 \leq \gamma \leq 1$, and $h \geq 0$ (the spectrum of \hat{H} is invariant under the substitution $h \rightarrow -h$).

For such a model, its ground state lies in the maximum spin sector $S = N/2$ [41, 42]. In the basis $\{|\uparrow\uparrow\rangle, |\uparrow\downarrow\rangle, |\downarrow\uparrow\rangle, |\downarrow\downarrow\rangle\}$, the two-spin reduced density matrix can be obtained as [43]

$$\rho_{ij} = \begin{pmatrix} v_1 & 0 & 0 & u \\ 0 & y & y & 0 \\ 0 & y & y & 0 \\ u & 0 & 0 & v_2 \end{pmatrix} \quad (5)$$

and its elements $v_{1,2}$, y , and u are given by

$$\begin{aligned} v_{1,2} &= \frac{N^2 - 2N + 4\langle S_z^2 \rangle \pm 4(N-1)\langle S_z \rangle}{4N(N-1)}, \\ y &= \frac{N^2 - 4\langle S_z^2 \rangle}{4N(N-1)}, \quad u = \frac{\langle S_x^2 \rangle - \langle S_y^2 \rangle}{N(N-1)}, \end{aligned} \quad (6)$$

where v_1 takes the plus sign and v_2 takes the minus sign (likewise for subsequent similar notation). The expectation values $\langle S_z \rangle$ and $\langle S_v^2 \rangle$ ($v = x, y, z$) could be obtained by virtue of different methods for the Hamiltonian (4) with different system parameters, and for $0 \leq \gamma \leq 1$ one also has $u \geq 0$ [41].

From Eq. (5) one can obtain directly that there is no single-spin coherence in the standard basis $\{|\uparrow\rangle, |\downarrow\rangle\}$ as $\rho_i = \text{tr}_j \rho_{ij}$ is diagonal. Of course, the resource theoretic measures of coherence are basis dependent [11], so the coherence of ρ_i measured with other bases can be nonzero. For example, the maximum l_1 norm and relative entropy of coherences attainable by optimizing the reference basis are given by [44]

$$C_{l_1}^{\max}(\rho_i) = |v_1 - v_2|, \quad C_r^{\max}(\rho_i) = 1 - H_2(v_1 + y), \quad (7)$$

where $H_2(\cdot)$ denotes the binary Shannon entropy function. For the two-spin state ρ_{ij} , the coherence can be obtained as

$$C_{l_1}(\rho_{ij}) = 2(y + u),$$

$$C_r(\rho_{ij}) = 2y + \sum_{i=1}^2 (\epsilon_i \log_2 \epsilon_i - v_i \log_2 v_i), \quad (8)$$

while the ASC and MSC can be obtained as (see Appendix A)

$$C_{l_1}^{\text{asc}}(\rho_{ij}) = \sum_{i=1}^2 \left(\frac{1}{2} x_i + |y - v_i| \right) + |y + u| + |y - u|,$$

$$C_r^{\text{asc}}(\rho_{ij}) = 2 + H_2(y + v_1) - \sum_{i=1}^2 \left[H_2\left(\frac{1 + x_i}{2}\right) + (y + v_i) H_2\left(\frac{y}{y + v_i}\right) \right], \quad (9)$$

$$C_{l_1}^{\text{msc}}(\rho_{ij}) = \frac{2(y + u)}{\sqrt{1 - (v_1 - v_2)^2}},$$

$$C_r^{\text{msc}}(\rho_{ij}) = H_2(r_{11}) - H_2\left(\frac{1 + \sqrt{(1 - 2r_{11})^2 + 4|r_{12}|^2}}{2}\right),$$

where the parameters $\epsilon_{1,2}$, $x_{1,2}$, r_{11} , and r_{12} are given by

$$\epsilon_{1,2} = \frac{1}{2} \left[v_1 + v_2 \pm \sqrt{4u^2 + (v_1 - v_2)^2} \right],$$

$$x_{1,2} = \sqrt{(v_1 - v_2)^2 + 4(y \pm u)^2}, \quad r_{12} = \frac{y + u}{\sqrt{1 - (v_1 - v_2)^2}}, \quad (10)$$

$$r_{11} = \frac{v_1}{1 + v_1 - v_2} + \frac{y}{1 - v_1 + v_2}.$$

Starting from the above analytical results, we explore in the following the performances of the coherence based indicators of the single- and two-spin reduced density matrices in signaling the occurrence of QPT in the LMG model.

IV. RESULTS

In the past few years, the quantum correlations in the LMG model, including the two-spin entanglement [45–48], entanglement entropy [49–51], multipartite entanglement [52–54], multipartite nonlocality [55], and quantum discord [56, 57], have been studied in depth in the context of QPTs. Moreover, the fidelity susceptibility [58, 59], quantum Fisher information [60], and the Loschmidt echo and fidelity [61] have also been widely studied.

As quantum coherence is a fundamental property of quantum states and reflects the origin of quantum correlations [20–24], it is natural to speculate that the quantum coherence may also play a vital role in the understanding of the quantum criticality in the high-dimensional systems. In particular, the two-spin entanglement in the LMG model decays rapidly with the increase of the system size N for any h and disappears in the large- N limit [42], while the calculation of the multipartite entanglement and nonlocality are intractable [52–55]. Quantum coherence and steered coherence for any two spins in the bulk, however, are not so sensitive to the increasing system size and are analytically solvable. Thereby, it is expected that they may discover useful information of the many-body systems. Motivated by these observations, we investigate in this section the coherence, ASC, and MSC in the LMG model and carry out a scaling analysis of their dependence on the system size N in different phase regions.

A. The thermodynamic limit

In the thermodynamic limit, a semiclassical approach gives the mean-field wave function [62, 63]

$$|\psi(\theta, \phi)\rangle = \bigotimes_{l=1}^N [\cos(\theta/2) e^{-i\phi/2} |\uparrow\rangle_l + \sin(\theta/2) e^{i\phi/2} |\downarrow\rangle_l], \quad (11)$$

with $|\uparrow\rangle_l$ and $|\downarrow\rangle_l$ the eigenstates of σ_z^l with eigenvalues 1 and -1 , respectively. Then one has

$$\langle \hat{H} \rangle = -\frac{(N-1)}{2} \sin^2 \theta (\cos^2 \phi + \gamma \sin^2 \phi) - hN \cos \theta, \quad (12)$$

and the ground state can be obtained by minimizing $\langle \hat{H} \rangle$ over θ and ϕ . For such a model, a second-order QPT occurs at the critical point $h = 1$. In the region of $h \geq 1$ (symmetric phase), the optimal angle $\theta_0 = 0$, all the spins are fully polarized in the direction of external magnetic field. In the region of $0 \leq h < 1$ (broken phase), $\theta_0 = \arccos h$, the ground state will be twofold degenerate ($\phi_0 = 0$ or π) for $\gamma \neq 1$ and infinitely degenerate (ϕ_0 can be arbitrary angle) for $\gamma = 1$.

We focus on $\gamma < 1$ (the case of $\gamma = 1$ is exactly solvable for any N and will be discussed in the next subsection). From Eq. (11) one can obtain that when $h \geq 1$, $v_1 = 1$, $v_2 = y = u = 0$. As a result, $C_\alpha(\rho_{ij}^T) = C_\alpha^{\text{msc}}(\rho_{ij}^T) = 0$ and $C_\alpha^{\text{asc}}(\rho_{ij}^T) = 2$ ($\alpha = l_1$ or r), where we have denoted by ρ_{ij}^T the two-spin density operator in the thermodynamic limit. Hence when the system is in the symmetric phase, the three quantumness measures always remain constant, which is understandable as all the spins are fully polarized in the magnetic field direction and the system's ground state is $|\uparrow\uparrow \dots \uparrow\rangle$. Moreover, at first glance, it seems contradictory for the MSC to be zero and the ASC to be finite in the symmetric phase. In fact, there is no contradiction because they are defined in different bases: One is in the eigenbasis of ρ_j which is state dependent and the other one is with respect to the three mutually unbiased bases.

When $0 \leq h < 1$, $v_{1,2} = h_\pm^2/4$ and $y = u = (1 - h^2)/4$, where we have defined $h_\pm = 1 \pm h$. Then, by making use of Eqs. (8),

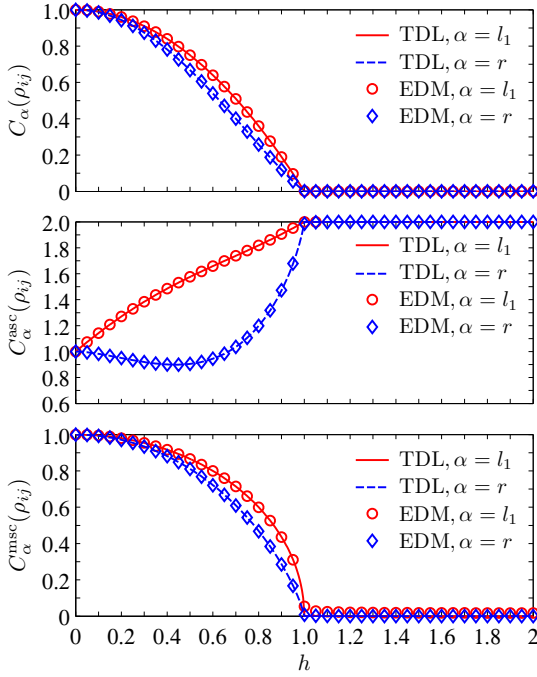


FIG. 1: Plot of $C_\alpha(\rho_{ij})$, $C_\alpha^{\text{asc}}(\rho_{ij})$, and $C_\alpha^{\text{msc}}(\rho_{ij})$ ($\alpha = l_1$ or r) versus h , where the solid lines denote the thermodynamic limit (TDL) results and the circles denote the exact diagonalization method (EDM) results with $\gamma = 0.5$ and $N = 2^{12}$.

(9), and (10), one can obtain

$$\begin{aligned}
 C_{l_1}(\rho_{ij}^T) &= [C_{l_1}^{\text{msc}}(\rho_{ij}^T)]^2 = 1 - h^2, \quad C_r^{\text{msc}}(\rho_{ij}^T) = H_2\left(\frac{h_+}{2}\right), \\
 C_r(\rho_{ij}^T) &= 1 + \frac{1+h^2}{2} \log_2(1+h^2) - \sum_{i=+,-} \frac{h_i^2 \log_2 h_i}{2}, \\
 C_{l_1}^{\text{asc}}(\rho_{ij}^T) &= \frac{1 - h^2 + 3h + \sqrt{1+h^4-h^2}}{2}, \\
 C_r^{\text{asc}}(\rho_{ij}^T) &= 2 - H_2\left(\frac{h_+}{2}\right) - H_2\left(\frac{1 + \sqrt{1+h^4-h^2}}{2}\right).
 \end{aligned} \tag{13}$$

In Fig. 1 we show h dependence of $C_\alpha(\rho_{ij})$, $C_\alpha^{\text{asc}}(\rho_{ij})$, and $C_\alpha^{\text{msc}}(\rho_{ij})$ for the thermodynamic limit result and the finite-size result of the exact diagonalization method. In the symmetric phase, as analyzed above, they always remain constant. In the broken phase, however, both $C_\alpha(\rho_{ij})$ and $C_\alpha^{\text{msc}}(\rho_{ij})$ ($\alpha = l_1$ or r) decrease with the increase of h , whereas $C_{l_1}^{\text{asc}}(\rho_{ij})$ increases with the increase of h , and $C_r^{\text{asc}}(\rho_{ij})$ first decreases to a minimum of about 0.8991 and then turns to be increased to 2. The coherence, ASC, and MSC could therefore be used as reliable indicators of QPT in this model. From Fig. 1 one can also note that the finite-size results with $N = 2^{12}$ are in good agreement with the mean-field results which are adaptive for the thermodynamic limit case. Similarly, for the single-spin state ρ_i , one has $C_\alpha^{\text{max}}(\rho_i^T) = 1$ ($\alpha = l_1$ or r) for $h \geq 1$, while $C_{l_1}^{\text{max}}(\rho_i^T) = h$ and $C_r^{\text{max}}(\rho_i^T) = 1 - H_2(h_+/2)$ for $0 \leq h < 1$. They also exhibit distinct behaviors in the two different phases.

B. The isotropic case

For the isotropic LMG model (i.e., $\gamma = 1$), due to the global symmetries described by $[\hat{H}, S^2] = 0$ and $[\hat{H}, S_z] = 0$, one has $\langle \hat{H} \rangle = 2M^2/N - 2hM - N/2$, with $M = \langle S_z \rangle$. By minimizing $\langle \hat{H} \rangle$ over all $M = -N/2, \dots, N/2$, one can obtain immediately the ground state as $|S, M_0\rangle$, with

$$M_0 = \begin{cases} N/2 & \text{for } h \geq 1, \\ I(hN/2) & \text{for } 0 \leq h < 1, \end{cases} \tag{14}$$

where $I(x)$ is the nearest integer (half-integer) from x for even (odd) N . When $h \geq 1$, $v_1 = 1$ and $v_2 = y = u = 0$, so one still has $C_\alpha(\rho_{ij}) = C_\alpha^{\text{msc}}(\rho_{ij}) = 0$ and $C_\alpha^{\text{asc}}(\rho_{ij}) = 2$ ($\alpha = l_1$ or r) in the symmetric phase region.

When $0 \leq h < 1$, by substituting M_0 into Eq. (6) and using $\langle S_x^2 \rangle = \langle S_y^2 \rangle$ for the ground state $|S, M_0\rangle$, one can obtain

$$\begin{aligned}
 C_{l_1}(\rho_{ij}) &= C_r(\rho_{ij}) = \frac{N_+ N_-}{2N(N-1)}, \quad C_{l_1}^{\text{msc}}(\rho_{ij}) = \frac{\sqrt{N_+ N_-}}{2N-2}, \\
 C_r^{\text{msc}}(\rho_{ij}) &= H_2\left(\frac{N_+ - 1}{2N-2}\right) - H_2\left(\frac{1}{2} + \frac{\sqrt{N^2 + 12M_0^2}}{4N-4}\right), \\
 C_{l_1}^{\text{asc}}(\rho_{ij}) &= x_0 + \frac{N_+ |1 - 2M_0| + N_- (N + 4M_0 + 1)}{2N(N-1)}, \\
 C_r^{\text{asc}}(\rho_{ij}) &= 2 - 2H_2\left(\frac{1+x}{2}\right) + H_2\left(\frac{N_+}{2N}\right) \\
 &\quad - \frac{N_+}{2N} H_2\left(\frac{N_-}{2N-2}\right) - \frac{N_-}{2N} H_2\left(\frac{N_+}{2N-2}\right),
 \end{aligned} \tag{15}$$

where we have denoted by $N_\pm = N \pm 2M_0$ and $x_0 = [N_+^2 N_-^2 + 16M_0^2(N-1)^2]^{1/2}/2N(N-1)$. From Eq. (15) one can obtain that for large N , the coherence, ASC, and MSC show qualitatively the same h dependence as those shown in Fig. 1.

C. Finite-size scaling

For the general LMG model with a finite number of spins, the expectation values $\langle S_z \rangle$ and $\langle S_\nu^2 \rangle$ ($\nu = x, y, z$) can be obtained approximately by means of the CUT method [64–66]. Different from the Holstein-Primakoff transformation method based on a first-order correction in the $1/N$ expansion of the spin operators, the CUT method takes into account the higher-order corrections and thus enables the extraction of the finite-size scaling exponents of different observables [41, 42]. In the following, we first figure out the scaling formulas of the ground-state coherence, ASC, and MSC with the help of the CUT results of $\langle S_z \rangle$ and $\langle S_\nu^2 \rangle$ ($\nu = x, y, z$) and then confirm them numerically using the exact diagonalization method with the system size up to $N = 2^{16}$.

First of all, we consider scaling behaviors at the QPT point. The expectation values of $\langle S_z \rangle$ and $\langle S_\nu^2 \rangle$ ($\nu = x, y, z$) obtained via the CUT technique can be found in Ref. [41]. For $h = 1$ with very large but finite N , by considering the fact that there should be no singularity for any physical quantity in a finite

TABLE I: Coefficients a_Φ ($\Phi = z, xx, yy, zz$) obtained numerically with $N = 2^{16}$ and different γ .

a_Φ	$\gamma = 0$	$\gamma = 0.25$	$\gamma = 0.50$	$\gamma = 0.75$
a_z	-0.4599	-0.4182	-0.3659	-0.2913
a_{xx}	0.9188	0.8354	0.7307	0.5813
a_{yy}	1.1144	1.2257	1.4017	1.7621
a_{zz}	-0.9195	-0.8362	-0.7315	-0.5824

system, one can obtain from Ref. [41] that

$$\begin{aligned} \frac{2\langle S_z \rangle}{N} &\sim 1 + \frac{1}{N} + \frac{a_z}{N^{2/3}}, \quad \frac{4\langle S_x^2 \rangle}{N^2} \sim \frac{a_{xx}}{N^{2/3}}, \\ \frac{4\langle S_y^2 \rangle}{N^2} &\sim \frac{a_{yy}}{N^{4/3}}, \quad \frac{4\langle S_z^2 \rangle}{N^2} \sim 1 + \frac{2}{N} + \frac{a_{zz}}{N^{2/3}}, \end{aligned} \quad (16)$$

where a_Φ ($\Phi = z, xx, yy, zz$) are the constants dependent on γ . Although their values cannot be determined with this scaling argument, we can obtain their approximate values by combining the above equation with the numerically obtained $\langle S_z \rangle$ and $\langle S_\nu^2 \rangle$ ($\nu = x, y, z$) with very large N ; see, e.g., the results listed in Table I, from which one can note that $a_{zz} \simeq 2a_z$. Hence, by combining Eq. (16) with Eq. (6) and neglecting the exponentially small terms in $1/N$, one can obtain

$$\begin{aligned} y + u &\sim \frac{a_{xx}}{2N^{2/3}}, \quad y - u \sim -\frac{1}{2N}, \\ y + v_1 &\sim 1 + \frac{a_z}{2N^{2/3}}, \quad y - v_1 \sim -1 - \frac{a_z + a_{zz}}{2N^{2/3}}, \\ y + v_2 &\sim -\frac{a_z}{2N^{2/3}}, \quad y - v_2 \sim \frac{a_z - a_{zz}}{2N^{2/3}}, \\ v_1 + v_2 &\sim 1 + \frac{a_{zz}}{2N^{2/3}}, \quad v_1 - v_2 \sim 1 + \frac{a_z}{N^{2/3}}. \end{aligned} \quad (17)$$

When considering the l_1 norm and relative entropy of coherence for the system at the critical point $h = 1$, as $v_1 - v_2 \gg u$ for very large N , one can obtain from Eq. (8) that

$$C_{l_1}(\rho_{ij}) \sim \frac{a_{xx}}{N^{2/3}}, \quad C_r(\rho_{ij}) \sim -\frac{a_{zz}}{2N^{2/3}}, \quad (18)$$

thus the coherence of the two-spin state scales as

$$\log_2[C_\alpha(\rho_{ij})] \sim -\frac{2}{3} \log_2 N + \text{const}, \quad (19)$$

where $\alpha = l_1$ or r , and the constant depends on α and γ (likewise for those subsequent scaling formulas in other phase regions). Such a scaling behavior could be verified by diagonalizing the Hamiltonian \hat{H} numerically in the spaces spanned by $\{|S, M_1\rangle\}$ ($M_1 = -N/2, -N/2 + 2, \dots, N/2$) and $\{|S, M_2\rangle\}$ ($M_2 = -N/2 + 1, -N/2 + 3, \dots, N/2 - 1$) in which the ground state lies. For the system size up to $N = 2^{16}$, we display in the topmost panel of Fig. 2 the numerical results, from which one can note that $\log_2[C_\alpha(\rho_{ij})]$ approaches the solid line with slope $-2/3$ with an increase in N .

For the ASC, by using the approximation $(1+x)^{1/2} \simeq 1+x/2$

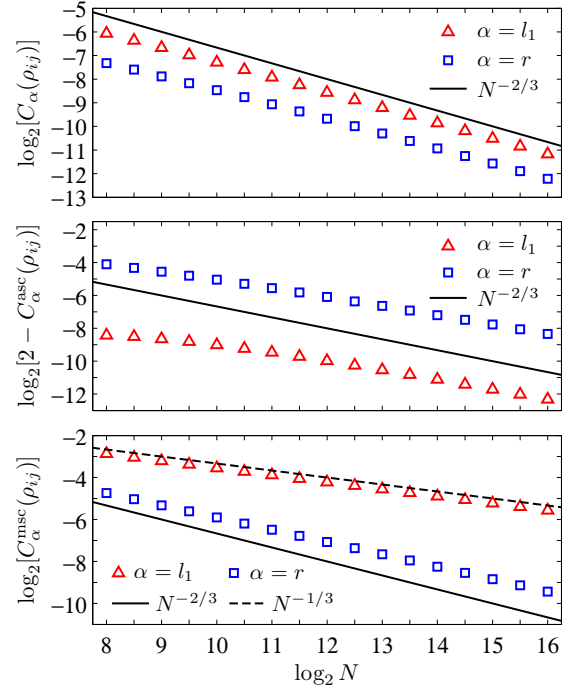


FIG. 2: Scaling behaviors of $C_\alpha(\rho_{ij})$, $C_\alpha^{\text{asc}}(\rho_{ij})$, and $C_\alpha^{\text{msc}}(\rho_{ij})$ ($\alpha = l_1$ or r) at the critical point $h = 1$ with $\gamma = 0.5$. The slopes of the solid and dashed lines are $-2/3$ and $-1/3$, respectively.

for very small x , one can obtain

$$\begin{aligned} x_{1,2} &\sim 1 + \frac{a_z}{N^{2/3}}, \quad \frac{y}{y + v_1} \sim -\frac{a_{zz}}{4N^{2/3}}, \\ \frac{y}{y + v_2} &\sim \frac{a_{zz}}{2a_z} + \frac{1}{a_z N^{1/3}}, \end{aligned} \quad (20)$$

and when the small x is positive, one also has $H_2(x) \simeq x/\ln 2$. These, together with Eqs. (9) and (17), yield

$$C_{l_1}^{\text{asc}}(\rho_{ij}) \sim 2 + \frac{4a_z + a_{xx}}{2N^{2/3}}, \quad C_r^{\text{asc}}(\rho_{ij}) \sim 2 + \frac{2a_z + a_{zz}}{4N^{2/3} \ln 2}, \quad (21)$$

where we have used the facts that $a_{xx} > 0$ and $a_{zz} \simeq 2a_z < 0$ (Table I). So the ASC has the finite-size scaling behavior

$$\log_2[2 - C_\alpha^{\text{asc}}(\rho_{ij})] \sim -\frac{2}{3} \log_2 N + \text{const}, \quad (22)$$

where $\alpha = l_1$ or r . This scaling formula was verified numerically by using the exact diagonalization method. As is shown in the middle panel of Fig. 2, the slope of $\log_2[2 - C_\alpha^{\text{asc}}(\rho_{ij})]$ approaches $-2/3$ gradually with an increase in N .

For the MSC, from Eqs. (10) and (17) one can obtain

$$r_{11} = \frac{a_{zz} + 2a_z}{4a_z} + \frac{a_{zz} + a_z}{4N^{2/3}}, \quad r_{12} = \frac{a_{xx}}{2\sqrt{-2a_z}N^{1/3}}, \quad (23)$$

then by substituting these into Eq. (9) and using the fact $a_{zz} \simeq 2a_z$, one can obtain

$$C_{l_1}^{\text{msc}}(\rho_{ij}) \sim \frac{a_{xx}}{\sqrt{-2a_z}N^{1/3}}, \quad C_r^{\text{msc}}(\rho_{ij}) \sim -\frac{a_{xx}^2}{4a_{zz}N^{2/3} \ln 2}, \quad (24)$$

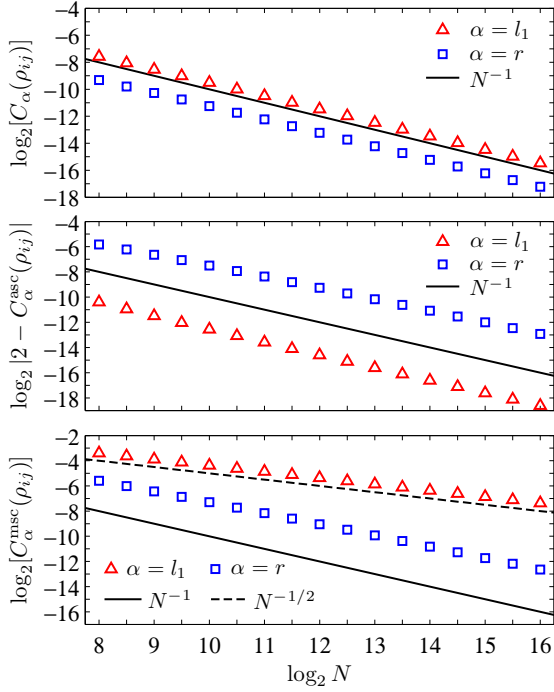


FIG. 3: Scaling behaviors of $C_\alpha(\rho_{ij})$, $C_\alpha^{\text{asc}}(\rho_{ij})$, and $C_\alpha^{\text{msc}}(\rho_{ij})$ ($\alpha = l_1$ or r) in the symmetric phase with $h = 1.1$ and $\gamma = 0.5$. The slopes of the solid and dashed lines are -1 and $-1/2$, respectively.

which indicate that the two forms of MSC scale as

$$\begin{aligned} \log_2[C_{l_1}^{\text{msc}}(\rho_{ij})] &\sim -\frac{1}{3} \log_2 N + \text{const}, \\ \log_2[C_r^{\text{msc}}(\rho_{ij})] &\sim -\frac{2}{3} \log_2 N + \text{const}, \end{aligned} \quad (25)$$

thus different from coherence and ASC, the scaling exponents for the two measures of MSC are different. These scaling behaviors have also been verified numerically. As shown in the bottommost panel of Fig. 2, with the increase of the system size N , the slopes of $\log_2[C_{l_1}^{\text{msc}}(\rho_{ij})]$ and $\log_2[C_r^{\text{msc}}(\rho_{ij})]$ approach $-1/3$ and $-2/3$, respectively.

Next, we consider scaling behaviors of the coherence, ASC, and MSC in the symmetric phase with $h > 1$. By defining $\Xi = (h-1)(h-\gamma)$, $\gamma_\pm = 1 \pm \gamma$, and neglecting the exponentially small terms in $1/N$, the CUT results of $\langle S_z \rangle$ and $\langle S_\nu^2 \rangle$ ($\nu = x, y, z$) can be written as [41]

$$\begin{aligned} \frac{2\langle S_z \rangle}{N} &\sim 1 + \frac{b_z}{N}, \quad \frac{4\langle S_x^2 \rangle}{N^2} \sim \frac{b_{xx}}{N}, \\ \frac{4\langle S_y^2 \rangle}{N^2} &\sim \frac{b_{yy}}{N}, \quad \frac{4\langle S_z^2 \rangle}{N^2} \sim 1 + \frac{b_{zz}}{N}, \end{aligned} \quad (26)$$

with $b_z = 1 + (\gamma_+ - 2h)/2\Xi^{1/2}$, $b_{xx} = (h - \gamma)/\Xi^{1/2}$, $b_{yy} = 1/b_{xx}$, and $b_{zz} = 2b_z$. Then, by combining Eq. (26) with Eqs. (6)–

(10) and after some algebra, one can obtain

$$\begin{aligned} C_{l_1}(\rho_{ij}) &\sim \frac{2b_0 - b_z}{N}, \quad C_r(\rho_{ij}) \sim -\frac{b_z}{N}, \\ C_{l_1}^{\text{asc}}(\rho_{ij}) &\sim 2 + \frac{2(b_0 + b_z)}{N}, \quad C_r^{\text{asc}}(\rho_{ij}) \sim 2 + \frac{b_z}{N \ln 2}, \\ C_{l_1}^{\text{msc}}(\rho_{ij}) &\sim \frac{2b_0 - b_z}{\sqrt{-2b_z} N^{1/2}}, \quad C_r^{\text{msc}}(\rho_{ij}) \sim -\frac{(2b_0 - b_z)^2}{8Nb_z \ln 2}, \end{aligned} \quad (27)$$

where we have defined $b_0 = b_{xx} - b_{yy}$ for the conciseness of Eq. (27). As $b_{xx} > 1$, $b_z < 0$, and $b_0 + b_z > 0$, one can find that

$$\begin{aligned} \log_2[C_\alpha(\rho_{ij})] &\sim -\log_2 N + \text{const}, \\ \log_2[C_{l_1}^{\text{asc}}(\rho_{ij}) - 2] &\sim -\log_2 N + \text{const}, \\ \log_2[2 - C_r^{\text{asc}}(\rho_{ij})] &\sim -\log_2 N + \text{const}, \\ \log_2[C_{l_1}^{\text{msc}}(\rho_{ij})] &\sim -\frac{1}{2} \log_2 N + \text{const}, \\ \log_2[C_r^{\text{msc}}(\rho_{ij})] &\sim -\log_2 N + \text{const}. \end{aligned} \quad (28)$$

Thus the scaling exponents for the two measures of coherence and ASC as well as that for the relative entropy of MSC are all -1 , whereas it is $-1/2$ for the l_1 norm of MSC, see also Fig. 3. This is different from those scaling exponents at the critical point $h = 1$. It indicates that with the increase of the system size N , $C_\alpha(\rho_{ij})$ and $C_\alpha^{\text{msc}}(\rho_{ij})$ in the region of $h > 1$ decrease faster than those at $h = 1$, while $C_r^{\text{asc}}(\rho_{ij})$ increases faster than that at $h = 1$. Moreover, $C_{l_1}^{\text{asc}}(\rho_{ij})$ decreases with the increase of N and approaches 2 in the thermodynamic limit, which is opposite to $C_{l_1}^{\text{msc}}(\rho_{ij})$ at the critical point.

Finally, by defining $\Lambda = 1 - h^2$ and neglecting those exponentially small terms in $1/N$, the CUT results of $\langle S_z \rangle$ and $\langle S_\nu^2 \rangle$ ($\nu = x, y, z$) in the broken phase can be obtained as [41]

$$\begin{aligned} \frac{2\langle S_z \rangle}{N} &\sim h + \frac{c_z}{N}, \quad \frac{4\langle S_x^2 \rangle}{N^2} \sim \Lambda + \frac{c_{xx}}{N}, \\ \frac{4\langle S_y^2 \rangle}{N^2} &\sim \frac{c_{yy}}{N}, \quad \frac{4\langle S_z^2 \rangle}{N^2} \sim h^2 + \frac{c_{zz}}{N}, \end{aligned} \quad (29)$$

with $c_z = h(\gamma_-/\Lambda)^{1/2}$, $c_{xx} = 2 + (\gamma h^2 + \gamma - 2)/(\Lambda \gamma_-)^{1/2}$, $c_{yy} = h/c_z$, and $c_{zz} = 2hc_z + (\Lambda \gamma_-)^{1/2}$. By combining Eq. (29) with Eqs. (6)–(10) and after some algebra, one can obtain

$$\begin{aligned} C_\alpha(\rho_{ij}) &\sim C_\alpha(\rho_{ij}^T) + \frac{a_\alpha}{N}, \quad C_\alpha^{\text{asc}}(\rho_{ij}) \sim C_\alpha^{\text{asc}}(\rho_{ij}^T) + \frac{b_\alpha}{N}, \\ C_\alpha^{\text{msc}}(\rho_{ij}) &\sim C_\alpha^{\text{msc}}(\rho_{ij}^T) + \frac{d_\alpha}{N}, \end{aligned} \quad (30)$$

where a_α , b_α , and d_α ($\alpha = l_1$ or r) are complicated polynomials of γ and h given by

$$\begin{aligned} a_{l_1} &= \frac{c_0 - c_{zz}}{2}, \quad b_{l_1} = \frac{\kappa_2 + 3c_z + c_0}{2}, \quad d_{l_1} = \frac{c_0 - c_{zz}}{2\sqrt{\Lambda}}, \\ a_r &= \frac{\kappa_1}{4} \left[\frac{1}{\ln 2} + \log_2 \left(\frac{1 + h^2}{2} \right) \right] - \frac{c_{zz}}{2} \left(1 + \frac{1}{\ln 2} \right) \\ &\quad + \frac{c_{zz} + 2c_z}{4} \log_2 \left(\frac{h_+^2}{4} \right) + \frac{c_{zz} - 2c_z}{4} \log_2 \left(\frac{h_-^2}{4} \right), \\ b_r &= \frac{\kappa_2}{2} \log_2 \left(\frac{\kappa_+}{\kappa_-} \right), \quad d_r = \kappa_3 \log_2 \left(\frac{h_-}{h_+} \right) + \frac{2\kappa_3 h + a_{l_1}}{2 \ln 2}, \end{aligned} \quad (31)$$

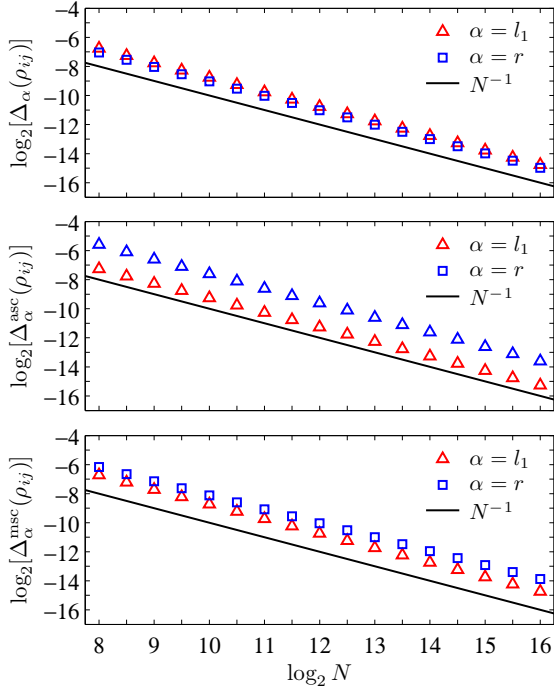


FIG. 4: Scaling behaviors of $C_\alpha(\rho_{ij})$, $C_\alpha^{\text{asc}}(\rho_{ij})$, and $C_\alpha^{\text{msc}}(\rho_{ij})$ ($\alpha = l_1$ or r) in the broken phase with $h = 0.9$ and $\gamma = 0.5$, where we have denoted by $\Delta_\alpha(\rho_{ij}) = C_\alpha(\rho_{ij}) - C_\alpha(\rho_{ij}^T)$, $\Delta_\alpha^{\text{asc}}(\rho_{ij}) = C_\alpha^{\text{asc}}(\rho_{ij}) - C_\alpha^{\text{asc}}(\rho_{ij}^T)$, and $\Delta_\alpha^{\text{msc}}(\rho_{ij}) = C_\alpha^{\text{msc}}(\rho_{ij}^T) - C_\alpha^{\text{msc}}(\rho_{ij})$ in this plot, and the slopes of the solid lines are -1 .

where $c_0 = c_{xx} - c_{yy}$, $\kappa_\pm = 1 \pm (\Lambda^2 + h^2)^{1/2}$, $\kappa_1 = c_{zz} + (\Lambda c_0 + 4hc_z)/(1 + h^2)$, $\kappa_2 = (hc_z + \Lambda a_l)/(\Lambda^2 + h^2)^{1/2}$, and $\kappa_3 = (2c_z - hc_{zz})/2\Lambda$. Thereby, the following scaling formulas hold:

$$\begin{aligned} \log_2[C_\alpha(\rho_{ij}^T) - C_\alpha(\rho_{ij})] &\sim -\log_2 N + \text{const}, \\ \log_2[C_\alpha^{\text{asc}}(\rho_{ij}) - C_\alpha^{\text{asc}}(\rho_{ij}^T)] &\sim -\log_2 N + \text{const}, \\ \log_2[C_\alpha^{\text{msc}}(\rho_{ij}^T) - C_\alpha^{\text{msc}}(\rho_{ij})] &\sim -\log_2 N + \text{const}. \end{aligned} \quad (32)$$

Thus the scaling exponents are always -1 in the broken phase, which are different from those at the QPT point. Such an observation has been confirmed by the numerical results shown in Fig. 4. It can be seen that the prediction of Eq. (32) works quite well. It also indicates that $C_\alpha(\rho_{ij})$ and $C_\alpha^{\text{msc}}(\rho_{ij})$ increase with the increase of the system size N and approach gradually their thermodynamic limit values of $C_\alpha(\rho_{ij}^T)$ and $C_\alpha^{\text{msc}}(\rho_{ij}^T)$, respectively, while $C_\alpha^{\text{asc}}(\rho_{ij})$ decreases with the increase of the system size N and approaches gradually $C_\alpha^{\text{asc}}(\rho_{ij}^T)$.

As the single-spin state ρ_i is concerned, it is straightforward to obtain from Eqs. (16), (26), and (29) that in the symmetric phase, the maximum attainable coherence scales as

$$\log_2[C_\alpha^{\text{max}}(\rho_i^T) - C_\alpha^{\text{max}}(\rho_i)] \sim s \log_2 N + \text{const}, \quad (33)$$

where $s = -2/3$ ($s = -1$) for $h = 1$ ($h > 1$), and in the broken phase it scales as

$$\log_2[C_\alpha^{\text{max}}(\rho_i) - C_\alpha^{\text{max}}(\rho_i^T)] \sim -\log_2 N + \text{const}. \quad (34)$$

Thus the scaling exponents for the maximum coherence of the single-spin state are completely the same as those for $\langle S_z \rangle/N$.

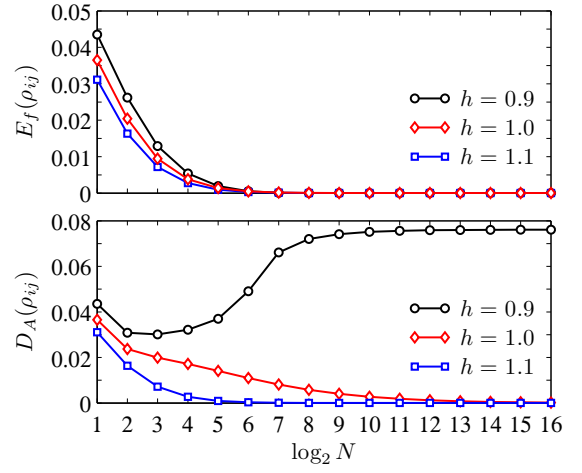


FIG. 5: Entanglement $E_f(\rho_{ij})$ and quantum discord $D_A(\rho_{ij})$ versus N with fixed $\gamma = 0.5$ and different h .

This is understandable as they are uniquely determined by the magnetization intensity $\langle S_z \rangle$.

Before ending this section, we provide a brief comparison of the performance of the coherence based indicators with the other quantum correlations, including entanglement of formation $E_f(\rho_{ij})$ [67, 68] and quantum discord $D_A(\rho_{ij})$ [69, 70] of ρ_{ij} . As is shown in Fig. 5, $E_f(\rho_{ij})$ decays rapidly with the increase of N and becomes extremely small after $N \gtrsim 2^6$, while for $D_A(\rho_{ij})$ it also decreases rapidly with the increase of N in the symmetric phase and approaches a very weak value in the broken phase. This may reduce their effectiveness in signaling the criticality of the LMG model as the accurate measurement of such weak quantities is a highly demanding task in experiments. But as what we have shown above, the coherence based indicators do not suffer from this problem, and this might be considered an advantage of them over entanglement and discord. Moreover, quantum coherence and ASC are analytically solvable for any state [11, 25], the coherence can be estimated with elaborately designed experiments [71, 72], and the measurement of ASC is also comparably simpler than that of entanglement and discord as it does not require a two-spin state tomography. Finally, the coherence based indicators are not so sensitive to the increasing system size N (they are finite even for infinite N) and the choice of two spins in the system. This property is also valuable as it removes the restriction on the necessity of a careful choice of two spins. Thus, the coherence based measures might serve as complementary indicators of quantum criticality in many-body systems.

V. SUMMARY AND DISCUSSION

To summarize, we have investigated the coherence, ASC, and MSC of the LMG model which undergoes a second-order QPT with the variation of the transverse magnetic field. The motivation for considering this problem lies in that coherence reflects the origin of quantumness and underlies various forms of quantum correlations, thus QPTs which correspond to dra-

matic changes of the ground state of a system, may be tied to the critical changes of the coherence based quantifiers. Moreover, the properties of the high-dimensional systems are rich compared to those one-dimensional ones in general, while the coherence based indicators are insensitive to the system size, thus they may be capable of capturing some key ingredients of the quantum criticality, especially for those in the regions with vanishing entanglement and discord. Thereby, it is worthy to present a thorough analysis of them.

We have obtained the analytical solutions of the coherence, ASC, and MSC for the thermodynamic limit and the isotropic cases of the LMG model, and analyzed in detail their properties by using the exact diagonalization method for the general anisotropic case. The results showed that they exhibit distinct behaviors in the symmetric and broken phases. These distinct behaviors could be identified as reliable indicators of quantum criticality in the LMG model. They also confirm that these coherence based indicators work well in signaling quantum criticality not only for the one-dimensional spin systems [14–19] but also for the high-dimensional systems.

We have also obtained finite-size scaling exponents for the coherence, ASC, and MSC by using the CUT method and confirmed them numerically with the system size up to $N = 2^{16}$. It is found that their dependence on N is also phase dependent. Specifically, the two measures of coherence and MSC as well as the relative entropy of ASC show opposite dependence on N in the broken and symmetric phases, whereas the l_1 norm of ASC shows opposite dependence on N at and beyond the QPT point. Moreover, the differences between their scaling exponents can be comprehend as follows. First, for the single-spin state, the maximum coherence is solely determined by $\langle S_z \rangle$, so the scaling exponent is in accord with that of $2\langle S_z \rangle/N$. Second, the coherence, ASC, and MSC for the two-spin state are determined by $\langle S_z \rangle$ and $\langle S_v^2 \rangle$ ($v = x, y, z$). In the broken phase and the symmetric phase with $h > 1$, the scaling exponents for $2\langle S_z \rangle/N$ and $4\langle S_v^2 \rangle/N^2$ are always -1 , while at the critical point $h = 1$, the scaling exponents for $2\langle S_z \rangle/N$ and $4\langle S_{x,z}^2 \rangle/N^2$ are $-2/3$ and that for $4\langle S_y^2 \rangle/N^2$ is $-4/3$ (this term can be neglected as it is much smaller than the other terms). These lead to the same scaling exponents for the two measures of coherence and ASC as well as the relative entropy of MSC as those of $2\langle S_z \rangle/N$ and $4\langle S_{x,z}^2 \rangle/N^2$. As for the l_1 norm of MSC, due to the square root in Eq. (9), its scaling exponent in the symmetric phase equals half of those for $2\langle S_z \rangle/N$ and $4\langle S_{x,z}^2 \rangle/N^2$, while in the broken phase, $1 - (v_1 - v_2)^2 \sim \Lambda$, thus its scaling exponent is still the same as those for $2\langle S_z \rangle/N$ and $4\langle S_v^2 \rangle/N^2$. Physically, the l_1 norm of ASC shows a different dependence on N from the other coherence based indicators and the l_1 norm of MSC does not recover the underlying critical exponents of $2\langle S_z \rangle/N$ and $4\langle S_v^2 \rangle/N^2$ in the symmetric phase having their roots in the l_1 norm of coherence given in Eq. (1) as it neglects the diagonal elements of ρ_{ij} . In this sense, we argue that the relative entropy of coherence based indicators is more beneficial for studying the quantum criticality.

While the information uncovered by coherence and steered coherence may provide alternative perspective for understanding the quantum criticality in the LMG model, one might also concern the experimental verification of the connections be-

tween QPTs and coherence based indicators established here. For this purpose, one may resort to the progress on simulating the LMG model in trapped ions [35, 36], nitrogen-vacancy center ensembles [37], and superconducting qubits [38]. In particular, the dynamical phase transition in the LMG model has been experimentally demonstrated in a quantum simulator with all-to-all connected superconducting qubits [38]. Hence, it is possible to expect verification of these connections in future experiments with similar platforms. Moreover, the coherence based indicators require no prior knowledge of the order parameters; thus it is also of great interest to use them to study the exotic quantum phases in many-body systems such as the topological ordered phase without any local order parameter [73–75]. Additionally, the coherence based indicators are finite for almost all states (e.g., the ASC vanishes only for the maximally mixed state), even when discord is absent [10], so it is also appealing to use them to study the quantum criticality in the parameter regions without entanglement and discord, e.g., the factorization phenomenon which corresponds to the occurrence of a fully factorized ground state at certain critical driving system parameters [14, 18, 76–78].

ACKNOWLEDGMENTS

This work was supported by the National Natural Science Foundation of China (Grant Nos. 11675129 and 11934018), the Strategic Priority Research Program of Chinese Academy of Sciences (Grant No. XDB28000000), and Beijing Natural Science Foundation (Grant No. Z200009).

Appendix A: Derivation of the MSC

As the reduced density operator $\rho_j = \text{tr}_i \rho_{ij}$ is nondegenerate for $h \neq 0$, one only needs to take the maximization over the set of projective measurements $M = (\mathbb{1} + \vec{m} \cdot \vec{\sigma})/2$ (see [29] for an explanation), where $\vec{\sigma} = (\sigma_x, \sigma_y, \sigma_z)$ is a vector composed of the Pauli operators and \vec{m} is a unit vector in \mathbb{R}^3 with the polar and azimuthal angles denoted by ϑ and φ , respectively.

For $C_{l_1}^{\text{asc}}(\rho_{ij})$, from Ref. [29] one can obtain

$$C_{l_1}^{\text{asc}}(\rho_{ij}) = \max_{\{\vartheta, \varphi\}} \frac{\sqrt{T_{11}^2 \cos^2 \varphi + T_{22}^2 \sin^2 \varphi \sin^2 \vartheta}}{1 + (v_1 - v_2) \cos \vartheta}, \quad (\text{A1})$$

where $T_{mn} = \text{tr}(\rho_{ij} \sigma_m \otimes \sigma_n)$. It is direct to obtain that $T_{11} = 2(y + u)$ and $T_{22} = 2(y - u)$ (hence $T_{11}^2 > T_{22}^2$), and the optimal azimuthal angle is given by $\varphi_0 = 0$ or π . In addition, one can obtain directly the optimal polar angle as $\vartheta_0 = \arccos(v_2 - v_1)$. All these yield $C_{l_1}^{\text{asc}}(\rho_{ij})$ in Eq. (9).

For $C_r^{\text{asc}}(\rho_{ij})$, we derive its expression as follows. First, the eigenbasis of $\rho_j = \text{tr}_i \rho_{ij}$ is given by $\{|\uparrow\rangle, |\downarrow\rangle\}$. Within this basis, the postmeasurement state of spin j can be obtained as

$$\rho_{j|M} = \frac{1}{p_M} \begin{pmatrix} v_1 \cos^2 \frac{\vartheta}{2} + y \sin^2 \frac{\vartheta}{2} & \frac{\sin \vartheta}{2} (ue^{i\varphi} + ye^{-i\varphi}) \\ \frac{\sin \vartheta}{2} (ue^{-i\varphi} + ye^{i\varphi}) & v_2 \sin^2 \frac{\vartheta}{2} + y \cos^2 \frac{\vartheta}{2} \end{pmatrix}, \quad (\text{A2})$$

where $p_M = y + v_2 + (v_1 - v_2) \cos^2(\vartheta/2)$. Hence, according to its definition [29], the MSC is given by

$$C_r^{\text{asc}}(\rho_{ij}) = \max_{\{\vartheta, \varphi\}} \{S[(\rho_{j|M})_{\text{diag}}] - S(\rho_{j|M})\}. \quad (\text{A3})$$

Then after some algebra, one can obtain that the optimal polar

angle and azimuthal angle related to M are still given by $\vartheta_0 = \arccos(v_2 - v_1)$ and $\varphi_0 = \{0, \pi\}$, respectively. By inserting them into Eq. (A2), one can obtain the optimized $\rho_{j|M}$ (we denote by r_{mn} its element that lies in the m th row and n th column). Hence, we obtained $C_r^{\text{asc}}(\rho_{ij})$ given in Eq. (9).

-
- [1] S. Sachdev, *Quantum Phase Transitions* (Cambridge University Press, Cambridge, 2000).
- [2] A. Osterloh, L. Amico, G. Falci, and R. Fazio, *Nature (London)* **416**, 608 (2002).
- [3] T. J. Osborne and M. A. Nielsen, *Phys. Rev. A* **66**, 032110 (2002).
- [4] S. J. Gu, H. Q. Lin, and Y. Q. Li, *Phys. Rev. A* **68**, 042330 (2003).
- [5] S. J. Gu, G. S. Tian, and H. Q. Lin, *Phys. Rev. A* **71**, 052322 (2005).
- [6] L. Amico, R. Fazio, A. Osterloh, and V. Vedral, *Rev. Mod. Phys.* **80**, 517 (2008).
- [7] K. Modi, A. Brodutch, H. Cable, T. Paterek, and V. Vedral, *Rev. Mod. Phys.* **84**, 1655 (2012).
- [8] A. Bera, T. Das, D. Sadhukhan, S. S. Roy, A. Sen(De), and U. Sen, *Rep. Prog. Phys.* **81**, 024001 (2018).
- [9] T. Werlang, C. Trippe, G. A. P. Ribeiro, and G. Rigolin, *Phys. Rev. Lett.* **105**, 095702 (2010).
- [10] M. L. Hu, X. Hu, J. C. Wang, Y. Peng, Y. R. Zhang, and H. Fan, *Phys. Rep.* **762–764**, 1 (2018).
- [11] T. Baumgratz, M. Cramer, and M. B. Plenio, *Phys. Rev. Lett.* **113**, 140401 (2014).
- [12] A. Streltsov, G. Adesso, and M. B. Plenio, *Rev. Mod. Phys.* **89**, 041003 (2017).
- [13] J. J. Chen, J. Cui, Y. R. Zhang, and H. Fan, *Phys. Rev. A* **94**, 022112 (2016).
- [14] G. Karpat, B. Çakmak, and F. F. Fanchini, *Phys. Rev. B* **90**, 104431 (2014).
- [15] M. Qin, Z. Ren, and X. Zhang, *Phys. Rev. A* **98**, 012303 (2018).
- [16] S. G. Lei and P. Q. Tong, *Quantum Inf. Process.* **15**, 1811 (2016).
- [17] Y. C. Li and H. Q. Lin, *Sci. Rep.* **6**, 26365 (2016).
- [18] T. C. Yi, W. L. You, N. Wu, and A. M. Oleś, *Phys. Rev. B* **100**, 024423 (2019).
- [19] A. L. Malvezzi, G. Karpat, B. C. Çakmak, F. F. Fanchini, T. Debarba, and R. O. Vianna, *Phys. Rev. B* **93**, 184428 (2016).
- [20] A. Streltsov, U. Singh, H. S. Dhar, M. N. Bera, and G. Adesso, *Phys. Rev. Lett.* **115**, 020403 (2015).
- [21] X. Qi, T. Gao, and F. Yan, *J. Phys. A* **50**, 285301 (2017).
- [22] K. C. Tan, H. Kwon, C. Y. Park, and H. Jeong, *Phys. Rev. A* **94**, 022329 (2016).
- [23] Y. Yao, X. Xiao, L. Ge, and C. P. Sun, *Phys. Rev. A* **92**, 022112 (2015).
- [24] M. L. Hu and H. Fan, *Phys. Rev. A* **95**, 052106 (2017).
- [25] D. Mondal, T. Pramanik, and A. K. Pati, *Phys. Rev. A* **95**, 010301(R) (2017).
- [26] M. L. Hu and H. Fan, *Phys. Rev. A* **98**, 022312 (2018).
- [27] M. L. Hu, X. M. Wang, and H. Fan, *Phys. Rev. A* **98**, 032317 (2018).
- [28] X. Hu and H. Fan, *Sci. Rep.* **6**, 34380 (2016).
- [29] X. Hu, A. Milne, B. Zhang, and H. Fan, *Sci. Rep.* **6**, 19365 (2015).
- [30] M. L. Hu, Y. Y. Gao, and H. Fan, *Phys. Rev. A* **101**, 032305 (2020).
- [31] Y. X. Xie, *Phys. Status Solidi B* **258**, 2000322 (2021).
- [32] H. J. Lipkin, N. Meshkov, and A. J. Glick, *Nucl. Phys.* **62**, 188 (1965).
- [33] N. Meshkov, A. J. Glick, and H. J. Lipkin, *Nucl. Phys.* **62**, 199 (1965).
- [34] A. J. Glick, H. J. Lipkin, and N. Meshkov, *Nucl. Phys.* **62**, 211 (1965).
- [35] R. G. Unanyan and M. Fleischhauer, *Phys. Rev. Lett.* **90**, 133601 (2003).
- [36] A. Russomanno, F. Iemini, M. Dalmonte, and R. Fazio, *Phys. Rev. B* **95**, 214307 (2017).
- [37] Y. Zhou, S. L. Ma, B. Li, X. X. Li, F. L. Li, and P. B. Li, *Phys. Rev. A* **96**, 062333 (2017).
- [38] K. Xu, Z. H. Sun, W. Liu, Y. R. Zhang, H. Li, H. Dong, W. Ren, P. Zhang, F. Nori, D. Zheng, H. Fan, and H. Wang, *Sci. Adv.* **6**, eaba4935 (2020).
- [39] Y. C. Zhang, X. F. Zhou, X. Zhou, G. C. Guo, and Z. W. Zhou, *Phys. Rev. Lett.* **118**, 083604 (2017).
- [40] Y. C. Liu, Z. F. Xu, G. R. Jin, and L. You, *Phys. Rev. Lett.* **107**, 013601 (2011).
- [41] S. Dusuel and J. Vidal, *Phys. Rev. B* **71**, 224420 (2005).
- [42] S. Dusuel and J. Vidal, *Phys. Rev. Lett.* **93**, 237204 (2004).
- [43] X. Wang and K. Mølmer, *Eur. Phys. J. D* **18**, 385 (2002).
- [44] Y. Yao, G. H. Dong, L. Ge, M. Li, and C. P. Sun, *Phys. Rev. A* **94**, 062339 (2016).
- [45] J. Vidal, G. Palacios, and R. Mosseri, *Phys. Rev. A* **69**, 022107 (2004).
- [46] J. Vidal, R. Mosseri, and J. Dukelsky, *Phys. Rev. A* **69**, 054101 (2004).
- [47] J. Vidal, *Phys. Rev. A* **73**, 062318 (2006).
- [48] J. Vidal, G. Palacios, and C. Aslangul, *Phys. Rev. A* **70**, 062304 (2004).
- [49] J. I. Latorre, R. Orus, E. Rico, and J. Vidal, *Phys. Rev. A* **71**, 064101 (2005).
- [50] V. Popkov and M. Salerno, *Phys. Rev. A* **71**, 012301 (2005).
- [51] T. Barthel, S. Dusuel, and J. Vidal, *Phys. Rev. Lett.* **97**, 220402 (2006).
- [52] H. T. Cui, *Phys. Rev. A* **77**, 052105 (2008).
- [53] A. C. Lourenço, S. Calegari, T. O. Maciel, T. Debarba, G. T. Landi, and E. I. Duzzioni, *Phys. Rev. B* **101**, 054431 (2020).
- [54] R. Orús, S. Dusuel, and J. Vidal, *Phys. Rev. Lett.* **101**, 025701 (2008).
- [55] J. Bao, B. Guo, H. G. Cheng, M. Zhou, J. Fu, Y. C. Deng, and Z. Y. Sun, *Phys. Rev. A* **101**, 012110 (2020).
- [56] M. S. Sarandy, *Phys. Rev. A* **80**, 022108 (2009).
- [57] C. Wang, Y. Y. Zhang, and Q. H. Chen, *Phys. Rev. A* **85**, 052112 (2012).
- [58] H. M. Kwok, W. Q. Ning, S. J. Gu, and H. Q. Lin, *Phys. Rev. E* **78**, 032103 (2008).
- [59] J. Ma, L. Xu, H. N. Xiong, and X. Wang, *Phys. Rev. E* **78**, 051126 (2008).
- [60] J. Ma and X. Wang, *Phys. Rev. A* **80**, 012318 (2009).

- [61] Q. Wang, P. Wang, Y. Yang, and W. G. Wang, *Phys. Rev. A* **91**, 042102 (2015).
- [62] R. Botet, R. Jullien, and P. Pfeuty, *Phys. Rev. Lett.* **49**, 478 (1982).
- [63] R. Botet and R. Jullien, *Phys. Rev. B* **28**, 3955 (1983).
- [64] F. Wegner, *Ann. Phys. (Berlin)* **3**, 77 (1994).
- [65] S. D. Glazek and K. G. Wilson, *Phys. Rev. D* **48**, 5863 (1993).
- [66] S. D. Glazek and K. G. Wilson, *Phys. Rev. D* **49**, 4214 (1994).
- [67] C. H. Bennett, D. P. DiVincenzo, J. A. Smolin, and W. K. Wootters, *Phys. Rev. A* **54**, 3824 (1996).
- [68] W. K. Wootters, *Phys. Rev. Lett.* **80**, 2245 (1998).
- [69] H. Ollivier and W. H. Zurek, *Phys. Rev. Lett.* **88**, 017901 (2001).
- [70] L. Henderson and V. Vedral, *J. Phys. A* **34**, 6899 (2001).
- [71] Y. T. Wang, J. S. Tang, Z. Y. Wei, S. Yu, Z. J. Ke, X. Y. Xu, C. F. Li, and G. C. Guo, *Phys. Rev. Lett.* **118**, 020403 (2017).
- [72] K. D. Wu, A. Streltsov, B. Regula, G. Y. Xiang, C. F. Li, and G. C. Guo, *Adv. Quantum Technol.* **4**, 2100040 (2021).
- [73] A. Kitaev and J. Preskill, *Phys. Rev. Lett.* **96**, 110404 (2006).
- [74] A. Hamma, W. Zhang, S. Haas, and D. A. Lidar, *Phys. Rev. B* **77**, 155111 (2008).
- [75] F. Pollmann, A. M. Turner, E. Berg, and M. Oshikawa, *Phys. Rev. B* **81**, 064439 (2010).
- [76] T. Roscilde, P. Verrucchi, A. Fubini, S. Haas, and V. Tognetti, *Phys. Rev. Lett.* **94**, 147208 (2005).
- [77] S. M. Giampaolo, G. Adesso, and F. Illuminati, *Phys. Rev. Lett.* **104**, 207202 (2010).
- [78] S. M. Giampaolo, G. Adesso, and F. Illuminati, *Phys. Rev. B* **79**, 224434 (2009).